FOXO nuclear shuttling dynamics are stimulus-dependent and correspond with cell fate

Kathleen A. Lasick[a], Elizabeth Jose[a], Allison M. Samayoa[d], Lisa Shanks[a], Kelvin W. Pond[a,b,c], Curtis A. Thorne[b,c], and Andrew L. Paek[a,c,*]

[a]Department of Molecular and Cellular Biology and [b]Department of Cellular and Molecular Medicine, University of Arizona, Tucson, AZ 85721; [c]University of Arizona Cancer Center, Tucson, AZ 85724; [d]Cancer Biology Graduate Interdisciplinary Program, University of Arizona, Tucson, AZ 85719

ABSTRACT **FOXO transcription factors are regulators of cellular homeostasis linked to increased lifespan and tumor suppression. FOXOs are activated by diverse cell stresses including serum starvation and oxidative stress. FOXO activity is regulated through posttranslational modifications that control shuttling of FOXO proteins to the nucleus. In the nucleus, FOXOs up-regulate genes in multiple, often conflicting pathways, including cell-cycle arrest and apoptosis. How cells control FOXO activity to ensure the proper response for a given stress is an open question. Using quantitative immunofluorescence and live-cell imaging, we found that the dynamics of FOXO nuclear shuttling is stimulus-dependent and corresponds with cell fate. H_2O_2 treatment leads to an all-or-none response where some cells show no nuclear FOXO accumulation, while other cells show a strong nuclear FOXO signal. The time that FOXO remains in the nucleus increases with the dose and is linked with cell death. In contrast, serum starvation causes low-amplitude pulses of nuclear FOXO and predominantly results in cell-cycle arrest. The accumulation of FOXO in the nucleus is linked with low AKT activity for both H_2O_2 and serum starvation. Our findings suggest the dynamics of FOXO nuclear shuttling is one way in which the FOXO pathway dictates different cellular outcomes.**

Monitoring Editor
Tom Misteli
National Institutes of Health, NCI

Received: Jun 1, 2022
Revised: Jan 20, 2023
Accepted: Jan 27, 2023

INTRODUCTION

The forkhead box O (FOXO) proteins are a family of transcription factors (TFs) that regulate homeostasis at both the cellular and tissue levels and have an evolutionarily conserved role in longevity (Kenyon *et al.*, 1993; Timmers *et al.*, 2019). There are four different FOXO genes in humans: *FOXO1*, *FOXO3*, *FOXO4*, and *FOXO6*. FOXO proteins are activated in response to a number of cellular stresses, including growth factor deprivation, metabolic stress, and oxidative stress. Upon activation, FOXO TFs up-regulate the transcription of hundreds of genes with diverse biological functions, including cell-cycle arrest (p21, p27), ROS scavenging (SOD2, CAT), autophagy (Bnip3, ATF4), inhibition of FOXO activity (PI3K, EGFR, RICTOR), and apoptosis (Bim, PUMA; Webb *et al.*, 2016). The cellular consequences of FOXO activation are both stress- and cell type–specific. For example, during quiescence, FOXO proteins play a protective role, up-regulating ROS scavengers and autophagy genes that are required for the long-term viability of stem cells (Kops *et al.*, 2002). In contrast, FOXO activity following H_2O_2 treatment or oncogene inhibition can lead to cell death through the up-regulation of apoptotic genes (Lehtinen *et al.*, 2006; Bean *et al.*, 2013).

The conflicting outcomes of FOXO activation suggest a need for precise control of FOXO activity to ensure that the response is commensurate with the stress. An attractive model for how input/output specificity is achieved by FOXO TFs is the idea of a "FOXO code" (Calnan and Brunet, 2008). In this model, posttranslational modifications (PTMs) alter the binding of FOXOs to different cofactors that control the level of FOXO TFs or their binding to the promoters of specific target genes. There is a lot of evidence to support this model. FOXO proteins can be modified by dozens of PTMs, and a subset of these PTMs have been shown to alter FOXO target gene expression (Wang *et al.*, 2016). For example, SIRT1 can deacetylate

This article was published online ahead of print in MBoC in Press (http://www.molbiolcell.org/cgi/doi/10.1091/mbc.E22-05-0193) on February 3, 2023.

*Address correspondence to: Andrew L. Paek (apaek@email.arizona.edu).

Abbreviations used: NAC, N-acetylcysteine; PTMs, posttranslational modification; TFs, transcription factors.

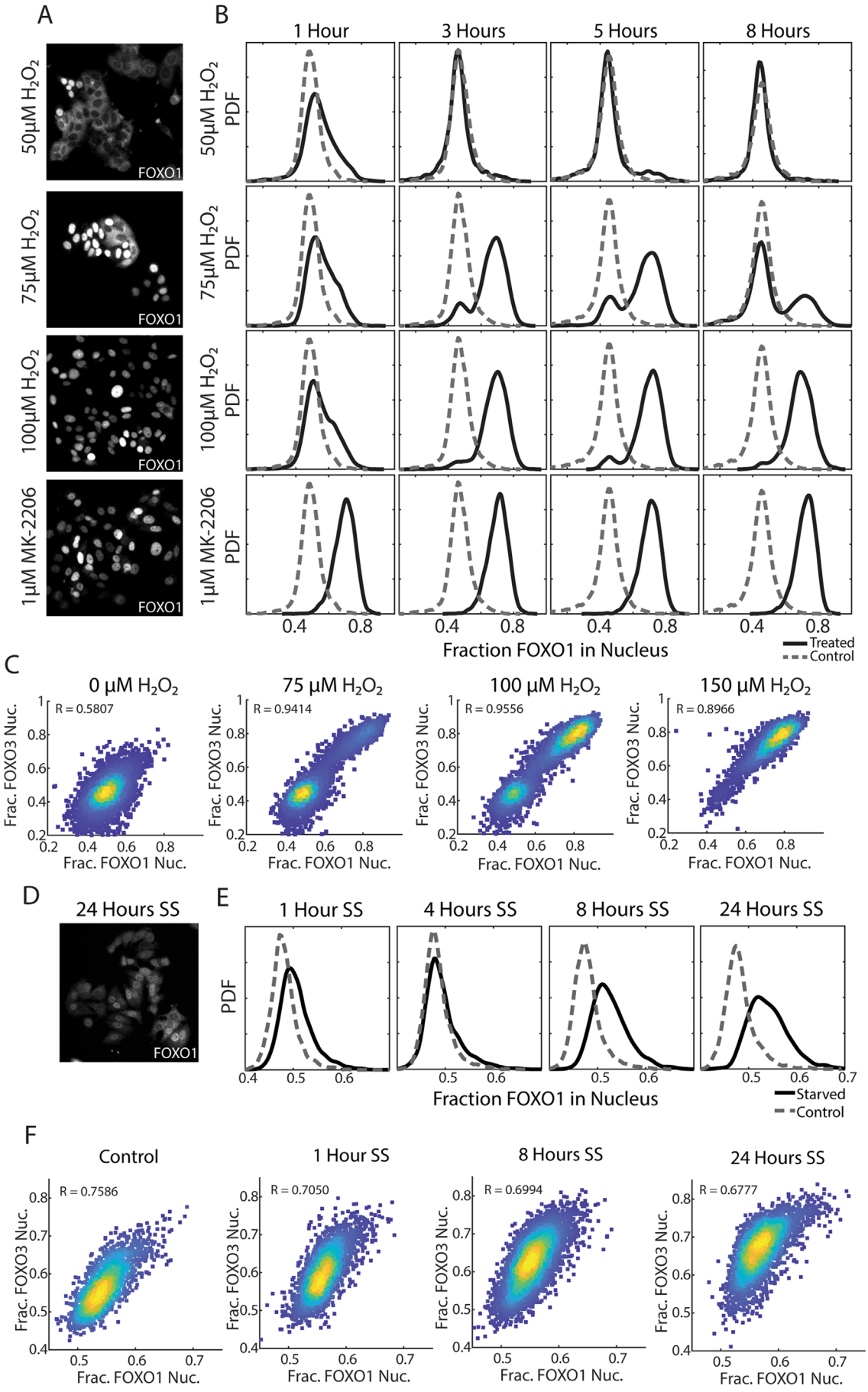
A
B
1 Hour
3 Hours
5 Hours
8 Hours
50μM H2O2
75μM H2O2
100μM H2O2
1μM MK-2206
FOXO1
PDF
Fraction FOXO1 in Nucleus
Treated
Control
C
0 μM H2O2
75 μM H2O2
100 μM H2O2
150 μM H2O2
R = 0.5807
R = 0.9414
R = 0.9556
R = 0.8966
Frac. FOXO3 Nuc.
Frac. FOXO1 Nuc.
D
24 Hours SS
E
1 Hour SS
4 Hours SS
8 Hours SS
24 Hours SS
Starved
Control
F
Control
1 Hour SS
8 Hours SS
24 Hours SS
R = 0.7586
R = 0.7050
R = 0.6994
R = 0.6777

FOXO proteins, and inhibition of SIRT1 increases the ability of ectopically expressed FOXO3 to induce cell-cycle arrest while inhibiting apoptosis (Brunet *et al.*, 2004). Moreover, mutations in the *FOXO1* gene that prevent acetylation lead to the uncoupling of weight gain and insulin resistance in mice (Banks *et al.*, 2011).

In addition to altering target gene specificity, FOXO PTMs likely provide an additional layer of control by altering the dynamics of FOXO TF shuttling in and out of the nucleus. FOXO TF activity is primarily regulated by nuclear/cytoplasmic shuttling by the regulation of AKT kinase activity (Tzivion *et al.*, 2011). Under progrowth conditions, AKT phosphorylates FOXO proteins at three serine/threonine residues (Brunet *et al.*, 1999). Phosphorylation at these sites sequesters FOXOs in the cytoplasm by inhibiting the FOXO nuclear localization signal, activating the nuclear export signal, and promoting the binding of FOXO to 14-3-3 proteins (Brunet *et al.*, 2002). Stresses activate FOXO by inhibiting AKT activity or through additional PTMs that prevent 14-3-3 binding and drive FOXO to the nucleus. Recent work has revealed that the dynamics of FOXO nuclear/cytoplasmic shuttling exhibits unique patterns that depend on treatment conditions. For example, when cells are serum-starved and then restimulated with different growth factors, FOXO1/FOXO3 shuttling to the cytoplasm shows growth factor–dependent dynamics. IGF1 induces sustained cytoplasmic FOXO, while other growth factors, including epiregulin and betacellulin, cause recurrent pulses of FOXO from the cytoplasm to the nucleus (Gross and Rotwein, 2015; Sampattavanich *et al.*, 2018). Pulses of FOXO nuclear/cytoplasmic shuttling have also been observed during energy stress induced by iodoacetate, an alkylating agent that inhibits GAPDH (Hung *et al.*, 2017). Similar patterns of stress-specific dynamics have been observed in other TFs, including p53, NF-KB, and MSN2, and have been linked to input/output specificity (Hoffmann *et al.*, 2002; Batchelor *et al.*, 2011; Hao and O'Shea, 2012; Purvis *et al.*, 2012; Paek *et al.*, 2016; Cheng *et al.*, 2021).

To determine the role of FOXO shuttling dynamics in the response to cellular stress, we used a combination of immunofluorescence and live-cell reporters to measure the temporal dynamics of FOXO1 and FOXO3 in response to H_2O_2-induced oxidative stress and serum starvation. These stresses were chosen due to the different FOXO–dependent cell outcomes they induce; H_2O_2 leads to FOXO–dependent cell death, while serum starvation largely results in FOXO–dependent arrest and protects cells from cellular senescence (Lehtinen *et al.*, 2006; Imai *et al.*, 2014). We focused on FOXO1 and FOXO3 due to the availability of good antibodies for staining and measuring their nuclear levels. We found that the dynamics of FOXO1/FOXO3 shuttling and cellular outcomes was stress-specific. In response to H_2O_2, FOXO enters the nucleus in a bimodal all-or-none manner: in some cells nearly all FOXO protein is in the nucleus, while other cells exhibit no accumulation of nuclear FOXO. For cells that show high levels of FOXO in the nucleus, it remains nuclear for either a short period of 4–5 h or an extended period of up to 48 h (though often shorter due to cell death). The fraction of cells with nuclear FOXO and the time it remained in the nucleus increased with the dose of H_2O_2 and was associated with more cell death. FOXO nuclear accumulation in response to H_2O_2 could be reversed by pretreating with the antioxidant N-acetylcysteine (NAC). However, adding NAC 2 h after H_2O_2 treatment had no effect on the FOXO response. Serum starvation, on the other hand, led to pulses of nuclear FOXO, with nuclear levels much lower than those measured in response to oxidative stress and fewer cell death events. Pulses of nuclear FOXO ceased rapidly after restimulation with serum. Differences in FOXO nuclear shuttling dynamics are reflected in the strength of AKT inhibition. H_2O_2 treatment results in a bimodal population of cells: one population with increased pAKT and low nuclear FOXO, and a separate population with low pAKT and high nuclear FOXO. In contrast, serum starvation causes graded levels of pAKT that are inversely correlated with nuclear FOXO levels.

RESULTS

The distribution of nuclear FOXO1 and FOXO3 is stress–specific

To determine if different stresses elicit different temporal dynamics of FOXO1 nuclear/cytoplasmic shuttling, we first performed an immunofluorescence time course of MCF7 cells exposed to increasing doses of H_2O_2 (Figure 1, A and B) or serum starvation (Figure 1, D and E) and measured the fraction of FOXO1 in the nucleus. The formula for calculating the nuclear fraction can be found in Supplemental Figure S1A. We observed a distinct pattern for each stress. H_2O_2 treatment elicited a bimodal staining pattern, in which some cells had mostly cytoplasmic FOXO1, similarly to untreated controls, while others had mostly nuclear FOXO1, similarly to cells treated with an AKT inhibitor (Figure 1B, bottom row). The proportion of cells with predominantly nuclear FOXO1 and their persistence over time increased with the H_2O_2 dose (Figure 1B). In contrast, serum withdrawal led to cells with a mix of nuclear and cytoplasmic FOXO1 with a wide unimodal distribution. The amount of nuclear FOXO1 increased slowly over time and peaked 24 h after serum withdrawal (Figure 1, D and E). To determine if these patterns are specific to FOXO1 or are shared by other isoforms, we costained cells with FOXO1 and FOXO3 antibodies. This revealed that the fractions of nuclear FOXO1 and FOXO3 were similar and correlated in individual cells (Figure 1, C and F; Supplemental Figure S1, C and F). We observed bimodal activation of FOXO1 in response to oxidative stress in the primary hTERT-immortalized human mammary epithelial cell line HME1 and in a two-dimensional human gut colonoid culture described recently, suggesting that this pattern of activation is not specific to MCF7 breast cancer cells (Supplemental Figure S1, B and E; Pond *et al.*, 2022). In addition, serum withdrawal led to a unimodal accumulation of nuclear FOXO1 in HME1 cells, similarly to the MCF7 data (Supplemental Figure S1D).

The duration of nuclear FOXO1 after H_2O_2 treatment is dose-dependent and associated with cell death

The distinct nuclear accumulation pattern for each stress suggests that dynamics might play a role in dictating different FOXO-induced

FIGURE 1: H_2O_2 and serum starvation induce different patterns of FOXO1/3 localization. (A) MCF7 cells were treated as labeled for 5 h, and then fixed and stained for FOXO1. (B) Distribution of the fraction of FOXO1 in the nucleus in MCF7 cells treated with H_2O_2 and MK-2206, an AKT inhibitor. (C) Density-colored scatterplots of the fractions of FOXO1 and FOXO3 in the nucleus in cells treated with the indicated concentrations of H_2O_2 for 5 h before fixation. (D) Sample image of MCF7 cells serum-starved (SS) for 24 h and stained for FOXO1. (E) Probability density function of the nuclear fraction of FOXO1 in MCF7 cells following serum starvation. (F) Density-colored scatterplots comparing the fractions of FOXO1 and FOXO3 in the nucleus in MCF7 cells serum-starved for the indicated numbers of hours before fixation. *R*-values in C and F are pairwise linear correlation coefficients.

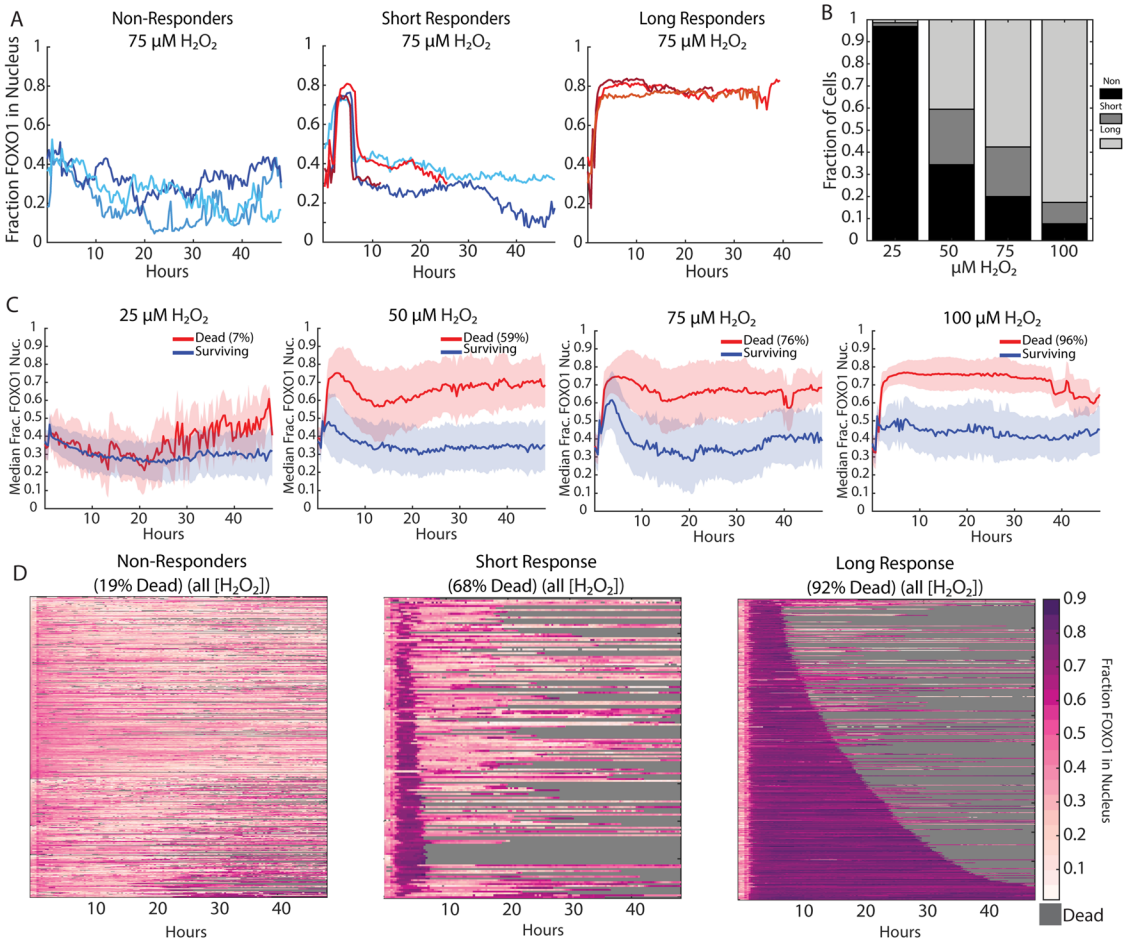

FIGURE 2: Accumulation of nuclear FOXO1 in response to H_2O_2 is all-or-none in single cells and linked with cell death. (A) Sample single-cell traces of fraction of FOXO1–Venus in the nucleus in response to 75 μM H_2O_2, separated by category of response: blue indicates surviving cells, red indicates dead cells. (B) Fractions of cells that were in each category by the concentration of H_2O_2 as indicated: 25 μM: $n = 294$, 50 μM: $n = 259$, 75 μM: $n = 276$, 100 μM: $n = 300$. (C) Median FOXO1 nuclear fraction in MCF7 cells that died (red) and survived (blue) H_2O_2 treatment. Shaded areas represent the median absolute deviation. (D) Heatmaps of all single-cell traces of fraction of FOXO1 in the nucleus, separated by the three categories demonstrated in A and sorted by the duration of the FOXO1 response. Gray indicates dead cells.

cell fates. To measure FOXO1 shuttling dynamics and cell-cycle arrest/death in single cells, we used a previously developed MCF7 cell line where CRISPR was used to add the Venus fluorescent protein to the C-terminus of FOXO1 and added an H2B-CFP tag for tracking nuclei (Stewart-Ornstein and Lahav, 2016). We verified that the distribution of nuclear accumulation of FOXO1 in response to H_2O_2, serum starvation, and AKT inhibition broadly matched the distributions observed by immunofluorescence of untagged FOXO1 (Figure 1, B and E; Supplemental Figure S2, A and B). However, the amplitude of the response was not as strong, possibly reflecting the decreased sensitivity of live-cell imaging as compared with immunofluorescence. In addition, there was an increase in the number of FOXO1 positive cells at 50 μM H_2O_2 (Figure 1, B and E; Supplemental Figure S2, A and B). This is likely due to the known sensitivity of the H_2O_2 response to cell number (Gülden *et al.*, 2010; Lim *et al.*, 2014).

We first looked at the dynamics of FOXO1 shuttling in response to H_2O_2. Cells were treated with four different doses of H_2O_2 and imaged every 20 min for 48 h (Supplemental Movie 1). Approximately 300 single cells were tracked for each dose, and we extracted the nuclear fraction of FOXO1-mVenus signal for each cell using previously developed software (Reyes *et al.*, 2018). Cell death events were detected by morphology. The average FOXO1–mVenus nuclear fraction increases with H_2O_2 dose, consistent with our immunofluorescence data (Supplemental Figure S2C).

We observed three broad patterns of nuclear FOXO1 accumulation in single cells. In the first pattern, which we call non responders, cells show no or only a brief pulse of nuclear FOXO1 (<1 h, Figure 2, A and D, Left panel), with the majority of these cells surviving H_2O_2 treatment. The second pattern, which we call short-responders, exhibits a 1–5-h pulse of high nuclear FOXO1 levels followed by a rapid and sustained switch to the cytoplasm; ~68% of these cells died (Figure 2, A and D, Middle). The final pattern, which we call long-responders, showed a sustained nuclear FOXO1 signal for long periods of time (>5 h, mean ~18 h) that ended in cell death in 92% of cells (Figure 2, A and D, Right panel; see Supplemental Figure S2E for correlation of FOXO1 duration and cell death). It is important to note that cells were sorted into each category based on the length of the initial FOXO1 pulse, and some cells that died reactivated FOXO1 at later time points, perhaps through H_2O_2-induced stress that takes longer to accumulate or H_2O_2-independent stresses. The fraction of cells showing a long nuclear FOXO1

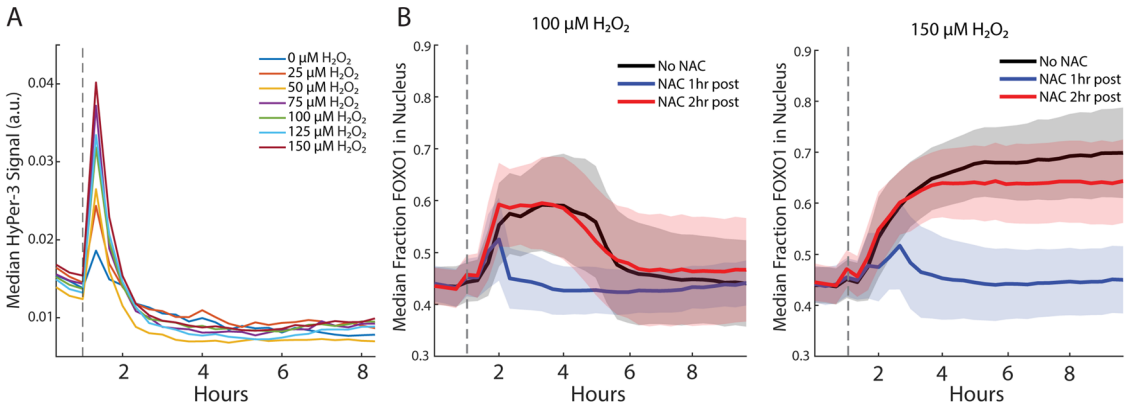

FIGURE 3: Accumulation of Nuclear FOXO1 shows time-dependent irreversibility. (A) Median Hyper-3 signal in MCF7 cells treated with different concentrations of H_2O_2. Dashed vertical line indicates time of H_2O_2 addition. (B) Median signal of the fraction of FOXO1 in the nucleus over time in cells treated with 100 μM (left) and 150 μM H_2O_2 (right), and then treated with NAC at the indicated times after H_2O_2 treatment. Dashed vertical line indicates time of H_2O_2 addition.

response increased with dose (Figure 2B). Additionally, the median trace of cells that survive H_2O_2 treatment exhibits both a lower amplitude and a shorter duration of nuclear FOXO1, and this pattern was consistent across H_2O_2 doses (Figure 2C).

The number of divisions a cell experienced after H_2O_2 treatment decreased with increasing dose, and even at lower doses, cells in the long responder category were less likely to divide again (Supplemental Figure S2D). Together, these data suggest that nuclear FOXO1 accumulation in response to H_2O_2 is all-or-none in single cells, and the time it remains in the nucleus increases with H_2O_2 dose. In addition, cells exhibit substantial heterogeneity in the time that FOXO1 remains in the nucleus, and cell death is correlated with the length of time that FOXO1 remains in the nucleus.

Accumulation of nuclear FOXO1 shows time-dependent irreversibility

The observation that H_2O_2 triggers an "all-or-none" nuclear accumulation of FOXO1 in single cells suggests that FOXO1 is controlled by a bistable system. One feature of bistable systems is that they exhibit hysteresis, meaning that the response of cells to a stimulus depends on whether the cell is in the on or off state. Cells in the off state require relatively high levels of stimulus to switch to the on state. In contrast, cells in the on state require relatively low levels of stimulus to maintain activation. At the extreme, bistable systems can show irreversibility, where the complete removal of the stimulus is insufficient for turning the system off (Ferrell, 2002). We hypothesized that nuclear accumulation of FOXO1 was irreversible, as previous measurements of H_2O_2 levels with single-cell sensors showed rapid clearance of H_2O_2 in less than 1 h, whereas nuclear accumulation of FOXO1 lasts several hours and in some cases days (Figure 2B; Ermakova *et al.*, 2014). Indeed, using the HyPer-3 H_2O_2 reporter, we found that the reporter returned to baseline levels in less than 1 h for all doses tested (Figure 3A; Bilan *et al.*, 2013).

To test whether the FOXO1 response exhibited hysteresis in response to H_2O_2, we used N-acetylcysteine (NAC), an antioxidant that rapidly reduces H_2O_2 and other reactive oxygen species (Pedre *et al.*, 2021). We first verified that pretreating cells with NAC prevented nuclear FOXO1 accumulation in response to H_2O_2 (Supplemental Figure S3A). We then performed a time-lapse experiment where cells were first treated with H_2O_2 and with NAC at different time points. While treatment with NAC 1 h after H_2O_2 causes FOXO1 to exit the nucleus and accumulate in the cytoplasm, adding NAC 2 h after treatment is no longer capable of reversing the FOXO1 response (Figure 3B). This indicates that the nuclear accumulation of FOXO1 shows time-dependent irreversibility and that H_2O_2 is no longer needed to maintain nuclear FOXO1 2 h after treatment.

FOXO1 shows a reversible pulsatile activation pattern in response to serum starvation

We next measured the dynamics of FOXO1–mVenus shuttling in response to serum starvation. MCF7 FOXO1–mVenus H2B–ECFP cells were imaged every 20 min for 125 h. For the first 5 h, cells were grown in 5% serum to get a baseline, after which the level of serum was dropped from 5% to 0.02%, and cells were imaged for 72 h and then restimulated with 2% serum to determine if the FOXO1 response was reversible (Supplemental Movie 2).

Example single-cell traces can be seen in Figure 4A. In response to serum withdrawal, cells exhibit a synchronized short spike in nuclear FOXO1 that lasts ~20–30 min, after which FOXO1 returns to the cytoplasm. FOXO1 then reenters the nucleus after a delay that varies from cell to cell (14.9 ± 13.7 h); in some cells FOXO1 returns to the nucleus within a few hours, while other cells require more than 24 h for FOXO1 to return to the nucleus (Figure 4B). The median trace of all cells predominantly reflects the fraction of cells in which FOXO1 has returned to the nucleus (Figure 4C). Once FOXO1 returns to the nucleus, it begins a series of pulses in and out of the nucleus for the remainder of the time that cells are under serum withdrawal conditions (Figure 4, A and B). In response to serum withdrawal, cells slow cell divisions and ~32% of cells die. The concentration of FOXO1 in the nucleus was higher in apoptotic cells than in surviving cells, yet the fraction of total FOXO1 levels in the nucleus was similar between the two populations (Supplemental Figure S4, A and B). Interestingly, FOXO1 exits the nucleus rapidly upon restimulation with 2% FBS, which is associated with a rapid decline in cell death and a slower increase in mitotic events (Figure 4, C–E). Together, these data show that the FOXO1 response to serum withdrawal is different from that to H_2O_2 treatment. While H_2O_2 leads to an all-or-none accumulation of nuclear Foxo1 with time- dependent irreversibility, serum withdrawal causes stochastic pulses of nuclear FOXO1 that are rapidly reversible.

We next tested how H_2O_2 and serum starvation impact gene expression. We measured expression of two FOXO target genes

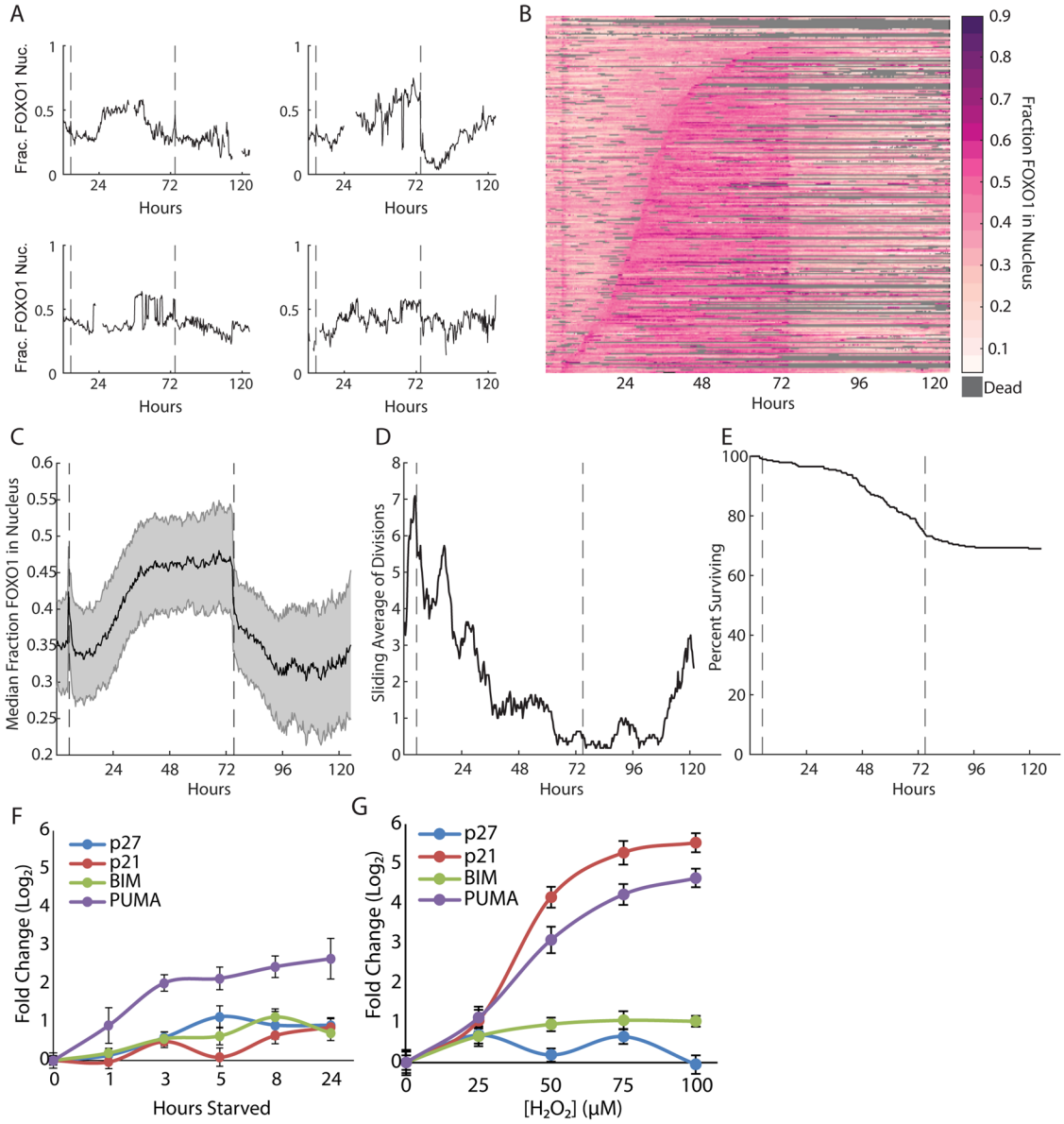

FIGURE 4: Serum starvation leads to pulsatile nuclear FOXO1 accumulation that is rapidly reversible. (A) Sample single-cell traces of fraction of FOXO1–mVenus in the nucleus over time after serum starvation and serum restimulation. The first dashed vertical line indicates a change from 5% FBS to 0.02% FBS medium; the second dashed vertical line indicates restimulation, a change from 0.02% FBS to 2% FBS medium. (B) Heatmap of 287 single-cell traces of the fraction of FOXO1–mVenus in the nucleus, sorted by time spent above a threshold of 0.45. (C) Median fraction of FOXO1–mVenus in the nucleus over time; shaded area indicates median absolute deviation. (D) Average number of divisions occurring over a 5-h sliding window. (E) Percentage of surviving cells over time. (F) qPCR fold change values for p27, p21, BIM, and PUMA RNA expression after the indicated hours of serum starvation in MCF7 cells. (G) qPCR fold change values for p27, p21, BIM, and PUMA RNA expression after 5 h of indicated concentrations of H_2O_2 in MCF7 cells.

involved in cell-cycle arrest (p21, p27) and two apoptotic target genes (BIM and PUMA). While expression of all four genes increased with both increasing duration of serum starvation (Figure 4F) and increasing concentration of H_2O_2 (Figure 4G), both PUMA and p21 levels were substantially higher in H_2O_2-treated cells than in serum-starved cells. These data allow a direct comparison of transcriptional activation of the FOXO targets after 5 h of treatment for both serum starvation and H_2O_2. For example, after 5 h of H_2O_2 treatment, PUMA levels increased 8–32 fold (50–100 μM), whereas 5 h of serum starvation led to a fourfold increase in PUMA levels. This is in line with the increased level and speed of cell death occurring after treatment with 50–100 μM H_2O_2 compared with after serum starvation.

The dynamics of FOXO1 shuttling in response to H_2O_2 and serum starvation are reflected by the strength of AKT inhibition

What accounts for the different dynamic patterns in cells treated with H_2O_2 and in serum-starved cells? Since AKT phosphorylation of FOXO is known to keep FOXOs in the cytoplasm, we sought to

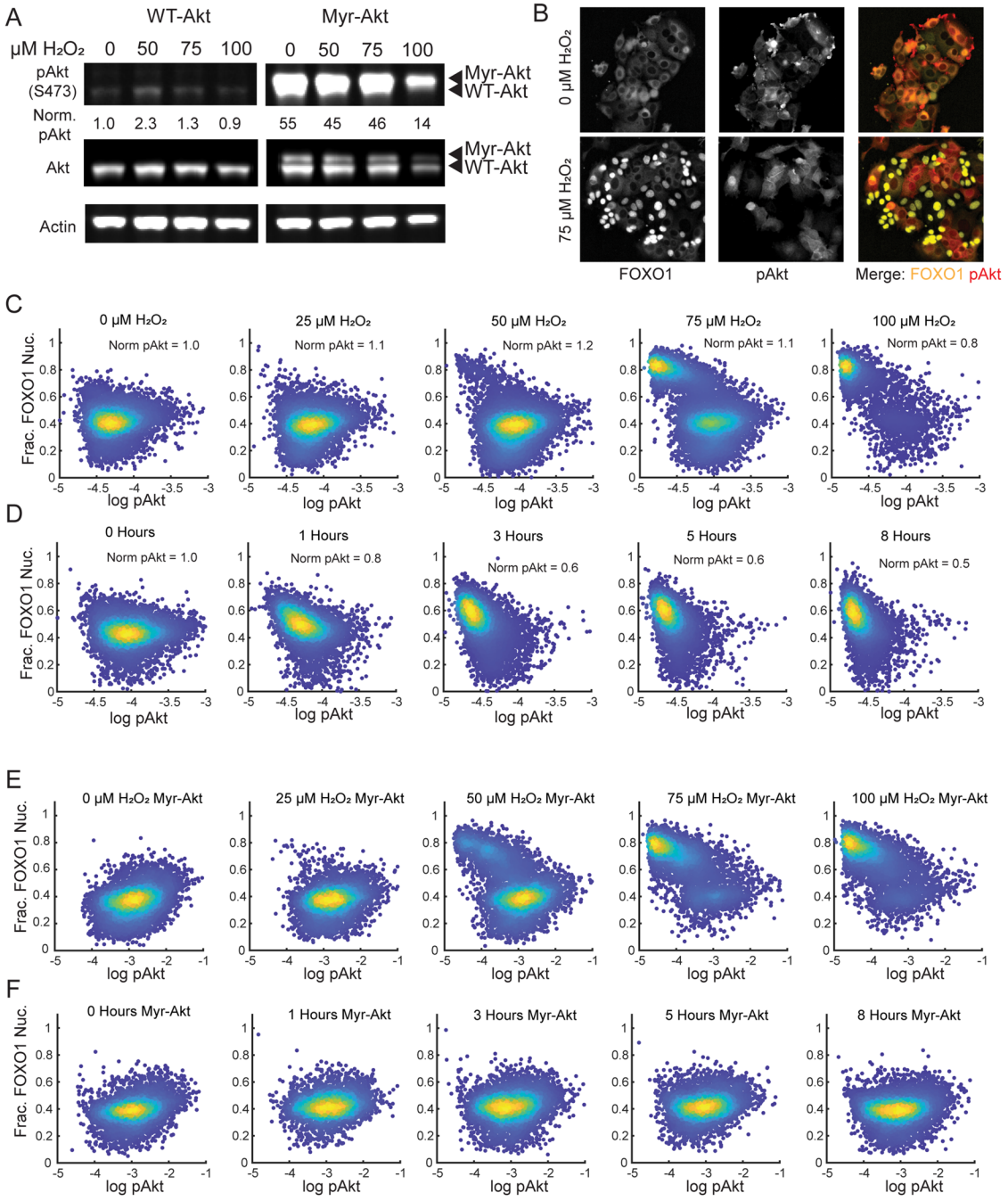

FIGURE 5: AKT is inactivated in cells with nuclear FOXO1. (A) Western blot stained for pAKT-S473, total AKT, and actin in MCF7 cells (left) and MCF7 cells with myristoylated AKT (Myr-AKT, right), treated with H_2O_2 for 5 h. Quantification of pAkt levels is indicated and normalized to pAKT of untreated cells without myr-AKT. Images are from the same blot but cropped between WT-Akt and Myr-Akt for clarity. (B) Sample images of MCF7 cells expressing FOXO1–mVenus, stained for pAKT-S473, fixed after no treatment or 5 h of 75 μM H_2O_2. (C, D) Scatterplots of the immunofluorescent pAKT-S473 signal and the fraction of FOXO1–mVenus in the nucleus after treatment with H_2O_2 for 5 h in MCF7 cells, C, or serum starvation over time in MCF7 cells, D. (E, F) Scatterplots of the immunofluorescent pAKT-S473 signal and the nuclear fraction of FOXO1 in MCF7 cells expressing myr-AKT after treatment with H_2O_2 for 5 h, E, or serum starvation over time, F.

determine whether a decrease in AKT activity was responsible for the bimodal activation of FOXO1 in response to H_2O_2. We first measured phosphorylation of AKT at serine 473 (pAKT-S473), a marker for AKT activity, by Western blot. H_2O_2 treatment led to a slight increase at lower concentrations but little change over untreated cells at higher concentrations (Figure 5A). The increase in pAKT-S473 is likely due to the activation of receptor tyrosine kinases by H_2O_2 (Sundaresan *et al.*, 1995; Heppner and van der Vliet, 2016; Dustin *et al.*, 2020).

The Western blot data suggested that AKT remained active in cells treated with H_2O_2. Yet given the cell-to-cell heterogeneity in FOXO1 accumulation, coupled with the increase in pAKT-S473 at

low levels of H_2O_2, it is possible that the Western blot data are misleading due to averaging cell populations. Indeed previous studies have shown that high levels of H_2O_2 can inhibit AKT (Martín *et al.*, 2002; Murata *et al.*, 2003). To test if AKT was active in cells with nuclear FOXO1, we measured both pAKT-S473 and FOXO1 nuclear accumulation by immunofluorescence in single cells following H_2O_2 treatment. Strikingly, these data revealed that cells with high nuclear FOXO1 levels showed low levels of pAKT-S473, while cells with cytoplasmic FOXO1 showed pAKT-S473 levels higher than those in untreated controls (Figure 5, B and C). Averaging the pAKT-S473 levels of the immunofluorescence data revealed a modest decrease at high levels of H_2O_2 due to the existence of the two different cell populations: cells with low pAKT-S473 and nuclear FOXO1 and cells with increased pAKT473 and cytoplasmic FOXO1 (Figure 5C). Note that some cells had high levels of pAKT-S473 and nuclear FOXO1 (Figure 5C, 75 μM). These cells are likely in a transition state, where AKT is being reactivated and FOXO1 is in the process of movement to the cytoplasm. In line with this, there was a downward slope in this cell population, consistent with these cells being in the process of transitioning from low AKT activity and nuclear FOXO1 to high AKT activity and cytoplasmic FOXO1. Moreover, the fraction of these cells decreased with H_2O_2 dose when fewer cells are expected to be making the transition between states. The density plots for FOXO1 and pAKT-473 can be seen individually in Supplemental Figure S5A.

We also measured pAKT-473 and FOXO1 nuclear accumulation in response to serum starvation. In contrast to H_2O_2 treatment, serum starvation caused a graded decrease in pAKT-S473, with nuclear FOXO1 levels showing an inverse correlation with pAKT-S473 levels (Figure 5D). Consistent with previous data, nuclear FOXO1 increased, while pAKT-S473 decreased over time in response to serum starvation (Figure 5D; see Supplemental Figure S5B for individual distributions).

To further test whether AKT inhibition was required for H_2O_2-induced nuclear accumulation of FOXO1, we introduced a myristoylated AKT construct (Myr-AKT), which drives AKT to the membrane, leading to hyperactivation of AKT (Martz *et al.*, 2014). Western blots confirmed hyperactivation of AKT as measured by pAKT-S473 (Figure 5A). High levels of H_2O_2 slightly decreased pAKT-S473, yet the levels were still substantially higher than in control cells lacking the Myr-AKT construct (Figure 5A). Immunofluorescence experiments revealed that H_2O_2 was still capable of inducing nuclear FOXO1 accumulation, yet cells with nuclear accumulation of FOXO1 had reduced pAKT-S473 despite the presence of the Myr-AKT construct (Figure 5E; see Supplemental Figure S5C for individual distributions). This suggests that H_2O_2 is capable of inhibiting both wild-type AKT and the Myr-AKT construct. In contrast, serum starvation did not alter nuclear accumulation of FOXO1 or pAKT-S473 levels in cells harboring the Myr-AKT (Figure 5F; see Supplemental Figure S5D for individual distributions). Together these data suggest that the mechanisms of AKT inactivation are different under H_2O_2 and serum starvation conditions. H_2O_2 causes a bimodal response, with high pAKT-S473 and low nuclear FOXO1 levels in one population, while other cells have a robust decrease in pAKT-S473 and high nuclear FOXO1 levels. Interestingly, H_2O_2 can still inactivate Myr-AKT. In contrast, serum starvation causes graded inactivation of pAKT-S473 and nuclear FOXO1 accumulation that can be reversed completely by Myr-AKT.

DISCUSSION

TFs are often activated by multiple signals, and upon activation can up-regulate a number of downstream programs with different phenotypic outcomes. Which programs are activated typically depends on both the type and magnitude of the signal. This multiple-input, multiple-output structure is particularly common amongst TFs that respond to cellular stress, including p53, NF-κB, MSN2, and FOXO TFs.

One way in which these TFs achieve input/output specificity is through linking inputs to specific dynamic patterns of TF activation (Purvis *et al.*, 2013). For example, activation of p53 by DNA double-strand breaks leads to regular pulses of p53 accumulation with relatively stable amplitude and frequency, which typically leads to transient cell-cycle arrest or senescence (Purvis *et al.*, 2012). If p53 levels are sustained by pharmacological inhibition of Mdm2, this forces cells into senescence. In contrast, other DNA-damaging agents such as cisplatin cause a single pulse of p53 accumulation, and the rate of p53 accumulation is linked to cell death (Paek *et al.*, 2016). NF-κB and Msn2 also exhibit pulsatile or sustained activation that is stimulus-dependent and linked to the expression of downstream target genes (Hao and O'Shea, 2012; Hansen and O'Shea, 2016; Mitchell *et al.*, 2016; Cheng *et al.*, 2021).

By measuring the shuttling of FOXO1 and FOXO3 in single cells, we found that nuclear accumulation of these two TFs is also stimulus-dependent. H_2O_2 leads to an all-or-none accumulation of FOXO1/3 in single cells, while serum starvation results in weaker nuclear FOXO1/3 that pulses into and out of the nucleus. The low-amplitude pulses of nuclear FOXO induced by serum starvation predominantly resulted in cell-cycle arrest, while the high levels of nuclear FOXO after H_2O_2 were associated with cell-cycle arrest and high levels of cell death.

There are several mechanisms that could contribute to the difference in cell fates associated with H_2O_2 and serum starvation. The low levels of nuclear FOXO during serum starvation could be insufficient to induce cell death through preferential binding to other FOXO targets, or alternatively, FOXO could bind to apoptotic promoters and enhancers with similar strength, but the low levels of FOXO lead to insufficient up-regulation of apoptotic genes. In addition, up-regulation of apoptotic genes could require high nuclear levels of FOXO for long durations to disrupt nucleosomal histone–DNA interactions in the promoters/enhancers of apoptotic genes, as shown recently for Msn2 and NF-κB (Hao and O'Shea, 2012; Cheng *et al.*, 2021). This is consistent with the observation that the amount of cell death in response to H_2O_2 increased with the duration of nuclear FOXO1. In addition, FOXO1 has been shown to perturb nucleosome binding to a FOXO1 response element in vitro, suggesting that it can act as a pioneer factor (Hatta and Cirillo, 2007). However, genome-wide studies in human cells found that FOXO3 mostly increases the transcription of target genes already in an open chromatin state, arguing against FOXO TFs acting as pioneer factors (Eijkelenboom *et al.*, 2013a,b). It is also likely that FOXO could be modified in a stress-specific manner, either by post-translational modifications or by cofactor binding to selectively up-regulate specific target genes. In addition, some of the cell death events caused by H_2O_2 are likely independent of FOXO, as we observed cell death events that occurred well after FOXO1 was switched off at lower concentrations of H_2O_2. Although previous studies found a strong reduction of H_2O_2-nduced cell death events in FOXO knockouts, some death events remained (Lehtinen *et al.*, 2006; Yamagata *et al.*, 2008). p53 is also activated in response to H_2O_2, and induces apoptotic genes (Shi *et al.*, 2021; Hanson and Batchelor, 2022). However, p53 knockdown experiments in these studies showed mixed results in the effect of H_2O_2-induced cell death.

The two different dynamic patterns of FOXO1/3 shuttling are likely due to their different modes of activation. Nuclear accumulation of FOXO1 in response to both H_2O_2 and serum starvation was associated with low AKT activity, although the mechanism of AKT inhibition was likely different. The pulsatile accumulation of FOXO1 in response to serum starvation is also consistent with the many known mechanisms of negative feedback in the PI3K/AKT pathway (Manning and Toker, 2017; Mukherjee *et al.*, 2021). The all-or-none irreversible accumulation of FOXO1 and FOXO3 suggests positive feedback in the mode of activation, though it is not clear what the mechanism of positive feedback is. There is evidence that in the presence of high H_2O_2 levels, Cys-297 and Cys-311 of AKT form a disulfide bond that shuts off AKT kinase activity (Murata *et al.*, 2003). This direct inactivation of AKT could explain why myristolated AKT, which is normally constitutively active, is inhibited by high concentrations of H_2O_2. There are also several separate mechanisms that have been linked to nuclear FOXO accumulation by ROS, including activation of the stress-activated MAP kinases p38 and JNK, the mammalian Ste20-like kinases MST1/2, activation of the arginine methyltransferae PRMT1, and formation of a disulfide bond with the nuclear import proteins Importin-7 and Importin-8 (Essers *et al.*, 2004; Lehtinen *et al.*, 2006; Yamagata *et al.*, 2008; Putker *et al.*, 2015; Hopkins *et al.*, 2018).

MATERIALS AND METHODS

Request a protocol through *Bio-protocol*.

Cell culture

MCF7 breast cancer cells and HME-1 hTert primary breast epithelial cells were grown in RPMI containing 10% fetal bovine serum (FBS), 100 units/ml penicillin, 100 µg/ml streptomycin, and 25 ng/ml amphotericin B. When needed for selection, puromycin, neomycin, and hygromycin were used at final concentrations of 500 ng/ml, 400 µg/ml, and 50 µg/ml, respectively.

Cell treatments

H_2O_2 experiments were performed by serially diluting stock H_2O_2 in PBS, until at 10× the concentration desired for the experiment. The 10× H_2O_2 solution was added directly to media for a final concentration of 1×. The stock H_2O_2 (Fisher Scientific AAL13235AP) was replaced monthly. Serum starvation experiments were performed by removing media, rinsing with PBS, and then adding 0.2% FBS media. MK-2206 (ApexBio A3010) was used from a stock concentration of 25 mM diluted in PBS before being added to media.

Cell line construction

myr-FLAG-AKT1-pcw107 was a gift from David Sabatini and Kris Wood (Addgene plasmid 64606; http://n2t.net/addgene:64606; RRID:Addgene_64606) and was used to make the MCF7 myr-AKT line. The H2B-ECFP lentiviral plasmid was described previously (Chakrabarti *et al.*, 2018). Lentiviral production and infection was performed as described in a previous publication (Tiscornia *et al.*, 2006). The pC1-HyPer-3 plasmid was a gift from Vsevolod Belousov (Addgene plasmid 42131; http://n2t.net/addgene:42131; RRID:Addgene_42131).

Immunofluorescence

Cells were plated in glass-bottomed multiwell plates (CellVis), treated, and then fixed with 2% paraformaldehyde, permeabilized with 0.1% Triton X-100 in PBS, blocked with 2% BSA in PBS, and incubated with primary antibodies overnight at 4°C in 2% BSA and 0.1% Tween 20 in PBS. Secondary antibodies are incubated for 1 h at room temperature in 2% BSA and 0.1% Tween 20 in PBS, stained with DAPI, and imaged in PBS. FOXO1 primary antibody: Cell Signaling 2880S; FOXO3 primary antibody: Cell Signaling 2497. To obtain single-cell correlation data between FOXO1 and FOXO3, after the FOXO3 primary and secondary incubations, samples were incubated with Rabbit IgG (Millipore-Sigma), and then a conjugated version of the FOXO1 primary antibody was used. Nuclei were segmented and mean nuclear FOXO1 and FOXO3 intensities were measured using CellProfiler (McQuin *et al.*, 2018). To obtain cytoplasmic FOXO1/FOXO3, a ring three pixels wide was drawn around the nuclear mask and mean cytoplasmic FOXO1/FOXO3 was extracted using this mask. Plots were created using MATLAB.

Live-cell microscopy

Cells were plated in a glass-bottomed 24-well plate (CellVis) at ~5000 cells per well, and grown in Roswell Park Memorial Institute, 10% FBS, 100 units/ml penicillin, 100 µg/ml streptomycin, and 25 ng/ml amphotericin B for 48 h and then rinsed with PBS and given DMEM Fluorobrite (ThermoFisher) medium with 5% FBS, 100 units/ml penicillin, 100 µg/ml streptomycin, 25 ng/ml amphotericin B, and 1× Glutamax (ThermoFisher). Cells were imaged every 20 min for 48–125 h by a Nikon Eclipse Ti microscope. The Nikon Perfect focus system was used to maintain focus. An OKO labs incubation system was used to maintain humidity, 37°C, and 5% CO_2. H2B-CFP was imaged using the C-FL AT ECFP/Cerulean Filter Set (Chroma) for 20–40 ms. FOXO1–mVenus was imaged using (Chroma) ET-EYFP Filter Set for 600 ms. HyPer3 probe was imaged using C-FL AT EGFP/FITC/CY2/Alexa Fluor 488 Filter Set (Chroma) for 300 ms. Fluorescence imaging used the Lumencor SOLA light engine. Images were taken using the Hamamatsu ORCA-Flash 4.0 camera with 16-bit depth and 2 × 2 binning. Movies were analyzed using single cell tracking software in MATLAB (Reyes *et al.*, 2018).

Western blot

Cells were rinsed and covered with PBS, scraped off the plate, and spun down, the liquid was aspirated, and the cells were frozen in liquid nitrogen and stored at –80°C. Cells were then thawed on ice and lysed (25 mM Tris pH 7.6, 150 mM NaCl, 1% NP-40, 1% Na-deoxycholate, and 0/1% SDS in water + protease inhibitor cocktail [Sigma] + phosphatase inhibitor cocktail [Sigma-Aldrich] + okadaic acid + sodium fluoride). Sample protein concentrations were measured with a Bradford assay (Bio-Rad) and equal protein concentrations were run on NuPAGE 4–2% Bis–Tris gels (Invitrogen). Protein was transferred to a nitrocellulose membrane and incubated in blocking solution (PBS, 5% BSA, 0.1% Tween 20) for 30 min at room temperature. The membrane was incubated with primary antibodies in blocking solution at 4°C overnight, rinsed three times in PBS with 0.1% Tween 20, and then incubated in secondary antibody for 1 h at room temperature. Antibodies: total AKT (Cell Signaling), phosphorylated AKT at S473 (Cell Signaling), 680LT secondary (LICOR-IRDye), 800CW secondary (LICOR-IRDye), actin (Sigma). The blot was imaged on the LI-COR Odyssey.

Quantitative PCR

After treatment, cells were rinsed with PBS, trypsinized, spun down, and flash frozen in liquid nitrogen. RNA was extracted using the RNeasy mini-kit (Qiagen). RNA concentration was measured via absorbance at 260 nm. RNA was converted to a cDNA library using the High-Capacity cDNA reverse transcription kit (Applied Biosciences). Quantitative PCR was performed in triplicate on the qTOWER^3 (analytikjena) with SYBR green master mix (Applied Biosciences), 16.8 ng cDNA, and 100 nM primers. The primer

sequences used were p27 forward: TCTGAGGACACGCATTTGG, p27 reverse: TGTTCTGTTGGCTCTTTTGTTT, p21 forward: TGTCACTGTCTTGTACCCTTG, p21 reverse: GGCGTTTGGAGTGGTAGAA, BIM forward: TGGAGACGAGTTTAACGCTTAC, BIM reverse: CCGCAAAGAACCTGTCAATG, PUMA forward: CGACCTCAACGCACAGTACG, PUMA reverse: GGGTGCAGGCACCTAATTGG, actin forward: TGCAGAAAGAGATCACCGC, and actin reverse: CCGATCCACACCGAGTATTTG.

ACKNOWLEDGMENTS

We thank members of the Paek and Thorne labs for helpful comments and discussion. We also thank A. El-Kareh, J. Schroeder, T. Weinert, and G. Yao for feedback on the manuscript. This work was supported by National Institutes of Health Grants RO1GM130864 (A.P.), T32-GM008659 (K.L.), NIH T32-GM132008 (K.L.), T32-CA009213-43 (A.M.), and R01GM130864-03 (A.M.).

REFERENCES

Banks AS, Kim-Muller JY, Mastracci TL, Kofler NM, Qiang L, Haeusler RA, Jurczak MJ, Laznik D, Heinrich G, Samuel VT, *et al.* (2011). Dissociation of the glucose and lipid regulatory functions of FoxO1 by targeted knockin of acetylation-defective alleles in mice. Cell Metab 14, 587–597.

Batchelor, E., Loewer, A., Mock, C., and Lahav, G (2011). Stimulus-dependent dynamics of p53 in single cells. Mol Syst Biol 7, 488.

Bean GR, Ganesan YT, Dong Y, Takeda S, Liu H, Chan PM, Huang Y, Chodosh LA, Zambetti GP, Hsieh JJ-D, *et al.* (2013). PUMA and BIM are required for oncogene inactivation-induced apoptosis. Sci Signal 6, ra20.

Bilan DS, Pase L, Joosen L, Gorokhovatsky AY, Ermakova YG, Gadella TWJ, Grabher C, Schultz C, Lukyanov S, Belousov VV (2013). HyPer-3: a genetically encoded H2O2 probe with improved performance for ratiometric and fluorescence lifetime imaging. ACS Chem Biol 8, 535–542.

Brunet A, Bonni A, Zigmond MJ, Lin MZ, Juo P, Hu LS, Anderson MJ, Arden KC, Blenis J, Greenberg ME (1999). AKT promotes cell survival by phosphorylating and inhibiting a Forkhead transcription factor. Cell 96, 857–868.

Brunet A, Kanai F, Stehn J, Xu J, Sarbassova D, Frangioni JV, Dalal SN, DeCaprio JA, Greenberg ME, Yaffe MB (2002). 14-3-3 transits to the nucleus and participates in dynamic nucleocytoplasmic transport. J Cell Biol 156, 817–828.

Brunet A, Sweeney LB, Sturgill JF, Chua KF, Greer PL, Lin Y, Tran H, Ross SE, Mostoslavsky R, Cohen HY, *et al.* (2004). Stress-dependent regulation of FOXO transcription factors by the SIRT1 deacetylase. Science 303, 2011–2015.

Calnan DR, Brunet A (2008). The FoxO code. Oncogene 27, 2276–2288.

Chakrabarti S, Paek AL, Reyes J, Lasick KA, Lahav G, Michor F (2018). Hidden heterogeneity and circadian-controlled cell fate inferred from single cell lineages. Nat Commun 9, 5372.

Cheng QJ, Ohta S, Sheu KM, Spreafico R, Adelaja A, Taylor B, Hoffmann A (2021). NF-κB dynamics determine the stimulus specificity of epigenomic reprogramming in macrophages. Science (80-) 372, 1349–1353.

Dustin CM, Heppner DE, Lin MCJ, Van Der Vliet A (2020). Redox regulation of tyrosine kinase signalling: more than meets the eye. J Biochem 167, 151–163.

Eijkelenboom A, Mokry M, De Wit E, Smits LM, Polderman PE, Van Triest MH, Van Boxtel R, Schulze A, De Laat W, Cuppen E, *et al.* (2013a). Genome-wide analysis of FOXO3 mediated transcription regulation through RNA polymerase II profiling. Mol Syst Biol 9, 638.

Eijkelenboom A, Mokry M, Smits LM, Nieuwenhuis EE, Burgering BMT (2013b). FOXO3 selectively amplifies enhancer activity to establish target gene regulation. Cell Rep 5, 1664–1678.

Ermakova YG, Bilan DS, Matlashov ME, Mishina NM, Markvicheva KN, Subach OM, Subach FV, Bogeski I, Hoth M, Enikolopov G, *et al.* (2014). Red fluorescent genetically encoded indicator for intracellular hydrogen peroxide. Nat Commun 5, 5222.

Essers MAG, Weijzen S, de Vries-Smits AMM, Saarloos I, de Ruiter ND, Bos JL, Burgering BMT (2004). FOXO transcription factor activation by oxidative stress mediated by the small GTPase Ral and JNK. EMBO J 23, 4802–4812.

Ferrell JE (2002). Self-perpetuating states in signal transduction: positive feedback, double-negative feedback and bistability. Curr Opin Cell Biol 14, 140–148.

Gross SM, Rotwein P (2015). AKT signaling dynamics in individual cells. J Cell Sci 128, 2509–2519.

Gülden M, Jess A, Kammann J, Maser E, Seibert H (2010). Cytotoxic potency of H_2O_2 in cell cultures: impact of cell concentration and exposure time. Free Radic Biol Med 49, 1298–1305.

Hansen AS, O'Shea EK (2016). Encoding four gene expression programs in the activation dynamics of a single transcription factor. Curr Biol 26, R269–R271.

Hanson RL, Batchelor E (2022). Coordination of MAPK and p53 dynamics in the cellular responses to DNA damage and oxidative stress. Mol Syst Biol 18, e11401.

Hao N, O'Shea EK (2012). Signal-dependent dynamics of transcription factor translocation controls gene expression. Nat Struct Mol Biol 19, 31–39.

Hatta M, Cirillo LA (2007). Chromatin opening and stable perturbation of core histone:DNA contacts by FoxO1. J Biol Chem 282, 35583–35593.

Heppner DE, van der Vliet A. (2016). Redox-dependent regulation of epidermal growth factor receptor signaling. Redox Biol 8, 24–27.

Hoffmann A, Levchenko A, Scott ML, Baltimore D (2002). The IκB-NF-κB signaling module: temporal control and selective gene activation. Science (80-) 298, 1241–1245.

Hopkins BL, Nadler M, Skoko JJ, Bertomeu T, Pelosi A, Shafaei PM, Levine K, Schempf A, Pennarun B, Yang B, *et al.* (2018). A peroxidase peroxiredoxin 1-specific redox regulation of the novel FOXO3 microRNA target let-7. Antioxidants Redox Signal 28, 62–77.

Hung YP, Teragawa C, Kosaisawe N, Gillies TE, Pargett M, Minguet M, Distor K, Rocha-Gregg BL, Coloff JL, Keibler MA, *et al.* (2017). AKT regulation of glycolysis mediates bioenergetic stability in epithelial cells. Elife 6, e27293.

Imai Y, Takahashi A, Hanyu A, Hori S, Sato S, Naka K, Hirao A, Ohtani N, Hara E (2014). Crosstalk between the Rb pathway and AKT signaling forms a quiescence–senescence switch. Cell Rep 7, 194–207.

Kenyon C, Chang J, Gensch E, Rudner A, Tabtiang R (1993). A *C. elegans* mutant that lives twice as long as wild type. Nature 366, 461–464.

Kops GJPL, Dansen TB, Polderman PE, Saarloos I, Wirtz KWA, Coffer PJ, Huang TT, Bos JL, Medema RH, Burgering BMT (2002). Forkhead transcription factor FOXO3a protects quiescent cells from oxidative stress. Nature 419, 316–321.

Lehtinen MK, Yuan Z, Boag PR, Yang Y, Villén J, Becker EBE, DiBacco S, de la Iglesia N, Gygi S, Blackwell TK, *et al.* (2006). A conserved MST-FOXO signaling pathway mediates oxidative-stress responses and extends life span. Cell 125, 987–1001.

Lim JB, Barker KA, Huang BK, Sikes HD (2014). In-depth characterization of the fluorescent signal of HyPer, a probe for hydrogen peroxide, in bacteria exposed to external oxidative stress. J Microbiol Methods 106, 33–39.

Manning BD, Toker A (2017). AKT/PKB signaling: navigating the network. Cell 169, 381–405.

Martín D, Salinas M, Fujita N, Tsuruo T, Cuadrado A (2002). Ceramide and reactive oxygen species generated by H_2O_2 induce caspase-3-independent degradation of AKT/protein kinase B. J Biol Chem 277, 42943–42952.

Martz CA, Ottina KA, Singleton KR, Jasper JS, Wardell SE, Peraza-Penton A, Anderson GR, Winter PS, Wang T, Alley HM, *et al.* (2014). Systematic identification of signaling pathways with potential to confer anticancer drug resistance. Sci Signal 7, ra121.

McQuin C, Goodman A, Chernyshev V, Kamentsky L, Cimini BA, Karhohs KW, Doan M, Ding L, Rafelski SM, Thirstrup D, *et al.* (2018). CellProfiler 3.0: next-generation image processing for biology.

Mitchell S, Vargas J, Hoffmann A (2016). Signaling via the NFκB system. Wiley Interdiscip Rev Syst Biol Med 8, 227–241.

Mukherjee R, Vanaja KG, Boyer JA, Gadal S, Solomon H, Chandarlapaty S, Levchenko A, Rosen N (2021). Regulation of PTEN translation by PI3K signaling maintains pathway homeostasis. Mol Cell 81, 708–723.e5.

Murata H, Ihara Y, Nakamura H, Yodoi J, Sumikawa K, Kondo T (2003). Glutaredoxin exerts an antiapoptotic effect by regulating the redox state of AKT. J Biol Chem 278, 50226–50233.

Paek AL, Liu JC, Loewer A, Forrester WC, Lahav G, Ahmed AU, Benetatos CA, Chunduru SK, Condon SM, McKinlay M, *et al.* (2016). Cell-to-cell variation in p53 dynamics leads to fractional killing. Cell 165, 631–642.

Pedre B, Barayeu U, Ezeri a D, Dick TP (2021). The mechanism of action of N-acetylcysteine (NAC): The emerging role of H_2S and sulfane sulfur species. Pharmacol Ther 228, 107916.

Pond KW, Morris JM, Alkhimenok O, Varghese RP, Cabel CR, Ellis NA, Chakrabarti J, Zavros Y, Merchant JL, Thorne CA, *et al.* (2022). Live-cell

imaging in human colonic monolayers reveals ERK waves limit the stem cell compartment to maintain epithelial homeostasis. eLife 11, 78837.
Purvis JE, Karhohs KW, Mock C, Batchelor E, Loewer A, Lahav G (2012). p53 dynamics control cell fate. Science 336, 1440–1444.
Purvis JE, Lahav G, Cohen AA, Reich-Zeliger S, Russ D, Shifrut E, Porat Z, Friedman N, Hoffmann A, Packman K, *et al.* (2013). Encoding and decoding cellular information through signaling dynamics. Cell 152, 945–956.
Putker M, Vos HR, Van Dorenmalen K, De Ruiter H, Duran AG, Snel B, Burgering BMT, Vermeulen M, Dansen TB (2015). Evolutionary acquisition of cysteines determines FOXO paralog-specific redox signaling. Antioxidants Redox Signal 22, 15–28.
Reyes J, Chen J-Y, Stewart-Ornstein J, Karhohs KW, Mock CS, Lahav G (2018). Fluctuations in p53 signaling allow escape from cell-cycle arrest. Mol Cell 71, 581–591.e5.
Sampattavanich S, Steiert B, Kramer BA, Gyori BM, Albeck JG, Sorger PK (2018). Encoding growth factor identity in the temporal dynamics of FOXO3 under the combinatorial control of ERK and AKT kinases. Cell Syst 6, 664–678.e9.
Shi T, van Soest DMK, Polderman PE, Burgering BMT, Dansen TB (2021). DNA damage and oxidant stress activate p53 through differential upstream signaling pathways. Free Radic Biol Med 172, 298–311.
Stewart-Ornstein J, Lahav G (2016). Dynamics of CDKN1A in single cells defined by an endogenous fluorescent tagging toolkit. Cell Rep 14, 1800–1811.
Sundaresan M, Yu ZX, Ferrans VJ, Irani K, Finkel T (1995). Requirement for generation of H_2O_2 for platelet-derived growth factor signal transduction. Science 270, 296–299.
Timmers PRHJ, Mounier N, Lall K, Fischer K, Ning Z, Feng X, Bretherick AD, Clark DW, Shen X, Esko T, *et al.* (2019). Genomics of 1 million parent lifespans implicates novel pathways and common diseases and distinguishes survival chances. Elife 8, 1–40.
Tiscornia G, Singer O, Verma IM (2006). Production and purification of lentiviral vectors. Nat Protoc 1, 241–245.
Tzivion G, Dobson M, Ramakrishnan G (2011). FoxO transcription factors; regulation by AKT and 14-3-3 proteins. Biochim Biophys Acta Mol Cell Res 1813, 1938–1945.
Wang Z, Yu T, Huang P (2016). Post-translational modifications of FOXO family proteins (Review). Mol Med Rep 14, 4931–4941.
Webb AE, Kundaje A, Brunet A (2016). Characterization of the direct targets of FOXO transcription factors throughout evolution. Aging Cell 15, 673–685.
Yamagata K, Daitoku H, Takahashi Y, Namiki K, Hisatake K, Kako K, Mukai H, Kasuya Y, Fukamizu A (2008). Arginine methylation of FOXO transcription factors inhibits their phosphorylation by AKT. Mol Cell 32, 221–231.